Colloids and Surfaces B: Biointerfaces 179 (2019) 199–207

Contents lists available at ScienceDirect

Colloids and Surfaces B: Biointerfaces

journal homepage: www.elsevier.com/locate/colsurfb

Surface lattice resonance of line array of poly (glycidyl methacrylate) with CdS quantum dots for label-free biosensing

Feng-Ping Lin[a,b], Hui-Ling Hsu[b], Chi-Jung Chang[c], Sheng-Chi Lee[d,**], Jem-Kun Chen[a,e,*]

[a] Department of Materials Science and Engineering, National Taiwan University of Science and Technology, 43, Sec 4, Keelung Rd., Taipei, 106, Taiwan, ROC
[b] Institute of Preventive Medicine, National Defense Medical Center, 161, Sec. 6, Minquan E. Rd., Neihu Dist., New Taipei City, Taiwan, ROC
[c] Department of Chemical Engineering, Feng Chia University, 100, Wenhwa Road, Seatwen, Taichung, 40724, Taiwan, ROC
[d] Department of Orthopediac Surgery, Pingtung Branch, Kaohsiung Veterans General Hospital, 1, Anping Lane 1, Zhao Sheng Road, Neibu Township, Pingtung County, Taiwan, ROC
[e] Applied Research Center for Thin-Film Metallic Glass, National Taiwan University of Science and Technology, Taipei, 10607, Taiwan, ROC

ARTICLE INFO

Keywords:
PGMA brush
Line arrays
CdS quantum dots
Line array

ABSTRACT

One dimensional plasmonic grating is a kind of resonant electromagnetic wave absorber with a characteristic wavelength. This study focusses on one-dimensional plasmonic grating consisting of poly (glycidyl methacrylate) (PGMA) brushes and CdS quantum dots (CdQDs) fabrication and PGMA chains grafted on a primary substrate in a line array continued by the immobilization of biotin-modified CdQDs. PGMA brush line array (PBLA) of plasmonic grating exhibited an absorptance at 441 nm while at the same time, CdQDs immobilized with PBLA showed characteristic absorbance at 396 nm. The blue-shift from 441 nm matches the absorbance peak of biotin-modified CdQDs resulting in the enhancement of photoluminescence emission of CdQDs. With streptavidin incubation to assemble CdQDs at 50 nM, the significant decrease in grating height resulted in the red-shift of the absorbance peak to 536 nm. Due to the deviation in absorbance, the intensity of the PL emission decreased gradually with the increase in concentration of streptavidin. In addition, our results showed that streptavidin incubation altered the color reflected from the surface due to effective changes in the refractive index of the layer as well. The limit of detection of the grating for streptavidin detection was determined to be 50 nM. Thus, PBLA-CdQD has the potential to act as a highly-sensitive, label-free optical biosensor.

1. Introduction

The strong exciton binding energy in quasi one-dimensional quantum dots (QD) enables quantum confinement [1]. The significant role of topology and geometrical parameters on the QD band structure and emission spectra has attracted considerable interest for practical device applications over the last 20 years. In particular, the promising applications of QDs in next generation display and lighting technology, such as QD-based light emitting diodes (QLEDs), have generated major research efforts [2,3]. Since the size, composition, and operational stability of QDs can be varied, the implantation of QDs in electroluminescence emitter devices provides narrow spectra with high color purity and tunable emission wavelengths [4,5]. CdS quantum dots (CdQDs) have also been extensively employed as absorber guests in various hybrid photoanodes for photoelectrochemical applications due to their suitable band structure and efficient visible light absorption [6,7].

Plasmonic nanostructures acting as optical antennae have been thoroughly investigated for different purposes in recent years, due to their abilities to focus light in subwavelength volumes and create strongly enhanced near fields on their surface. Such nanostructures demonstrate potential in applications in the areas of near-field optical microscopy and spectroscopy, biosensing, or light harvesting in optoelectronic devices [8,9]. Optical antennae can enhance the spontaneous emission or light absorption of organic molecules in their vicinity, which are related to their localized surface plasmon resonances (LSPRs) [10,11]. In chains or arrays of plasmonic nanostructures, collective grating-induced modes sometimes referred to as SLRs (surface lattice resonances), may also be present in addition to the LSPRs of single particles [10,12]. Plasmonic gratings have been combined with

* Corresponding author at: Department of Materials Science and Engineering, National Taiwan University of Science and Technology, 43, Sec 4, Keelung Rd., Taipei, 106, Taiwan, ROC.
** Corresponding author at: Department of Orthopediac Surgery, Pingtung Branch, Kaohsiung Veterans General Hospital, 1, Anping Lane 1, Zhao Sheng Road, Neibu Township, Pingtung County, Taiwan, ROC.
E-mail addresses: osclee.tw@msa.hinet.net (S.-C. Lee), jkchen@mail.ntust.edu.tw (J.-K. Chen).

https://doi.org/10.1016/j.colsurfb.2019.03.073
Received 20 January 2019; Received in revised form 21 March 2019; Accepted 31 March 2019
Available online 02 April 2019
0927-7765/ © 2019 Published by Elsevier B.V.

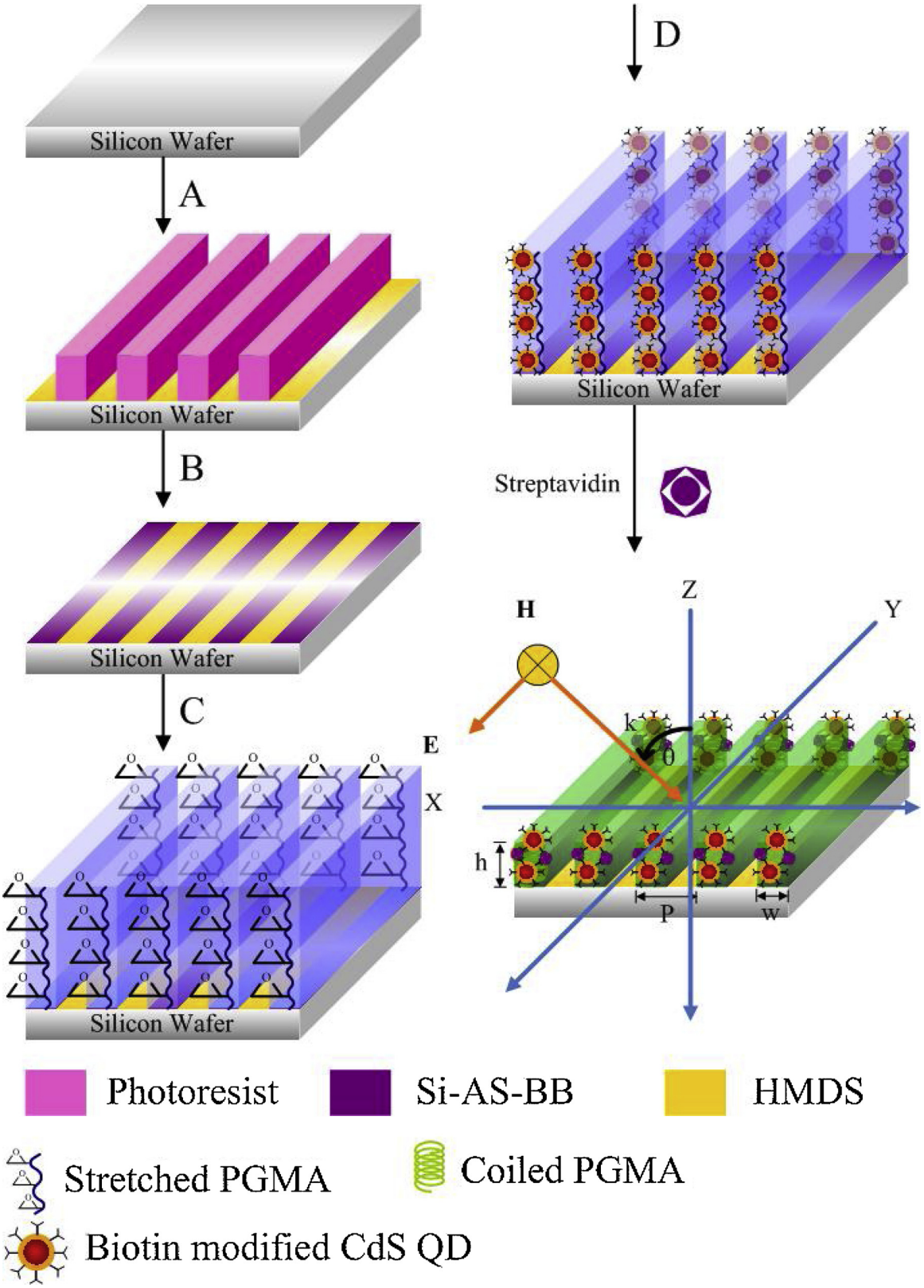

Fig. 1. Schematic illustration of the immobilization of CdQDs on PBLA on a surface. (Step A) Si wafer treated with HMDS in a thermal evaporator. Photoresist spin-coated onto the Si surface presenting $Si(CH_3)_3$ groups. I-line lithography used to pattern the photoresist with arrays of trenches on the surface. (Step B) AS selectively assembled onto regions of the trench arrays. BB selectively reacted with AS-treated Si surface to form the initiator. (Step C) Sample grafting through surface-initiated ATRP of GMA from the functionalized areas of the patterned initiator as plasmonic grating. (Step D) Immobilization of biotin modified CdQDs on the PBLA by covalent bonding exhibits streptavidin-responsive behavior on optical property.

organic dyes and semiconductors or dipolar emitters for experimental and theoretical study of spontaneous emission in coupled hybrid systems [13]. The emission of dye molecules can be strongly enhanced and directed in such systems when they undergo radioactive decay through the collective grating modes [14]. Furthermore, stimulated emission in such hybrid systems has also been observed [15]. In addition to emission enhancement, the coupling of lattice resonances to molecules has also been studied theoretically and experimentally [16,17]. However, investigation of plasmonic gratings combined with quantum dots in coupled hybrid systems and their optical properties has been rarely reported.

Polymer brushes belong to a class of polymer coating in which chains of the polymers are attached onto the substrate by covalent bonds [18,19]. Considerable robustness has been observed in the interfaces of these polymers as compared to the conventional coating techniques of spray, dip, and spin coating. Generally, these polymeric coatings can be attained by two methods, “grafting from” and “grafting to”. The second method produces surface-tethered polymers in “brush” conformation with high grafting density [20,21]. To date, the semiconductor process techniques utilized in several well-patterned polymer brushes have been fabricated to be used in photolithography [22,23], plasma etching [24,25], and atom transfer radical polymerization (ATRP) [26,27] to attain specific control over polymer brush composition, thickness, and patterns. Poly (glycidyl methacrylate) (PGMA) is a unique functional polymer, which can easily perform ring opening reactions with different functional groups ($-NH_2$, $-OH$, $-COOH$, and $-SH$) resulting in different functional PGMA derivatives. PGMA is a novel valuable polymeric brush due to its low-cost monomer source and excellent structural tenability, which can be controlled by radical polymerization reactions such as ATRP [28], and RAFT [29]. It has thus found usage in biochemistry and materials science as a surface linker [30]. PGMA and its abundant derivatives have displayed promising applications in gene and drug delivery, immunological assay, antibacterial agents, and enzyme immobilization [31,32]. In the present study, we grafted PGMA from silicon surface via ATRP as a line array of plasmonic grating to immobilize biotin-modified CdQDs. Plasmonic grating has been combined with quantum dots for an experimental study in coupled hybrid systems to enhance the optical properties of quantum dots. The gratings offer the advantage of plasmonic and lattice modes which can be tailored via their geometrical parameters, and spectrally tuned by the line height. The LSPRs of PGMA gratings both with and without CdQDs have been investigated by extinction spectra. Furthermore, the plasmonic grating is engineered to match the optical properties of the CdQDs in absorptance. Owing to the high bio-specificity between biotin and streptavidin, the CdQDs were modified with biotin to immobilize on the PGMA brush line array (PBLA) as an optical immunosorbent assay to detect streptavidin. Assembling the biotin-modified CdQDs on the PBLA after streptavidin incubation resulted in significant change in the extinction spectra. Surface plasmons of line array structure with QDs provide widespread opportunities in nanotechnological biosensor applications.

2. Materials and methods

One-hundred single-crystal silicon wafers in preferred orientation with the specifications of 5-inch diameter and ca.1.5 nm thick were supplied by Hitachi, Inc. (Japan). A sample of 2 cm × 2 cm size was cut from one side of the highly polished silicon wafer and used as a substrate for the experiments. 3-aminopropyltriethoxysilane (AS), 2-bromo-2-methylpropionyl bromide (BB), glycidyl methacrylate (GMA), triethylamine (TA), 1,1,4,7,7-pentamethyldiethylenetriamin (PMDETA), copper(I) bromide (Cu(I)Br), (copper(II) bromide) ($CuBr_2$), cadmium chloride hemi (pentahydrate), sodium sulfide nonahydrate and cysteamine (Acros Organics Co.) were used as reagents for graft polymerization and CdQDs synthesis. A vacuum distillation process was carried out for the chemicals GMA, PMDETA, AS, and BB prior to use. Reagent grade solvents and other chemicals needed for experiments were supplied by the Aldrich Chemical Co. and used without further purification. The procedure for removing dust particles and organic contaminants has been discussed in our previous report [33]. Biotin ($C_{10}H_{16}N_2O_3S$; MW: 244.31 g/mol, ≥99%), lyophilized powder, and streptavidin (lyophilized from 10 mM KH_2PO_4, ≥13 U/mg protein) were obtained from Sigma-Aldrich Corporation. AffiniPure goat anti-rabbit IgG (AGRI) was obtained from Jackson ImmunoResearch Lab. A 10 mM phosphate buffer containing 100 mM NaCl at pH 7.4 was prepared for the synthesis of 0.5 mM Sulfo-NHS-LC-LC-biotin and tested against serial dilutions of streptavidin. Milli-Q water (18.2 MΩ cm, Millipore Corp., Bedford, MA) was used for all experiments.

2.1. Patterning PGMA brushes as one-dimensional plasmonic grating

In our previous report [33], the technique of one dimensional plasmonic grating (line array) [34] patterned PGMA brushes fabrication procedure using very-large-scale integration (VLSI) process has been explained. Fig. 1 demonstrates the following various steps of the fabrication process: in step A, a 780 nm thick Si wafer previously spun with photoresist, is treated with hexamethyldisilazane. After that, the photoresist is patterned with a trench array using I-line lithography and allowed to develop. In step B, the Si substrate is immersed in a 0.5% (w/v) solution of AS in toluene at 50 °C for 2 h, for the purpose of ATRP initiator immobilization. It results in selective assembly of AS units onto the Si surface bare regions. The sample is then immersed sequentially in 2% (v/v) solutions of TA and BB at 20 °C for 8 h. The above steps produce the patterned surface of AS-BB for ATRP and photoresist areas. The remaining photoresist present in the HMDS-treated surface is removed by rinsing with solvent and results in chemically nanopatterned surface. In step C, ATRP reaction is followed by grafting the initiator-modified Si surface with the patterned PGMA brushes. PGMA brushes were then prepared on the surfaces of Si-AS-BB in the following manner: Cu(I)Br, $CuBr_2$, GMA, and PMDETA were added in 2:1 methanol-water solution and stirred at 90 °C in a de-oxygenated atmosphere with N_2 for 15 min, followed by addition of Si-AS-BB substrate. After polymerization for 24 h, a Soxhlet apparatus was used to remove unreacted catalyst, monomer, and non-grafted material. The modified surfaces were then dried under vacuum at 80 °C for 20 min. In step D, cysteamine capped CdQDs were prepared and characterized following the procedure detailed in a recent report [35]. Commercially available purified recombinant biotin was immobilized onto the prepared CdQD surface using EDC/NHS reaction [36]. The biotin-modified CdQDs were cleaned in an ultrasonic cleaner at 10 °C for various incubation times. The supernatant was decanted and the products were washed with PBS for at least three times to remove the residual biotin. The transmission electron microscopy (TEM) samples were prepared by evaporation of toluene solution droplets from the nanoparticles, on standard copper grids supported by holey carbon films. A lambda 25 spectrophotometer (Perkin Elmer) was used to measure UV–vis spectrum of the CdQDs of 4–5 nm diameter average particle size. The PGMA grafted samples were immersed in DMF in a round-bottom flask, with stirring. Excess biotin-modified CdQDs were used to initiate the reaction mixture by stirring for 12 h. CdQD-immobilized PBLA was obtained and denoted as PBLA-CdQD. The repetitive rinsing of the samples with DMF ensures removal of non- or weakly adsorbed particles. The products were removed from the solution by washing with diethyl ether. The final products were dried for 24 h in a vacuum oven, for future use. The prepared samples were incubated with streptavidin at various concentrations, for 2 h. The fundamental response of the optical properties of PBLA-CdQD was tested using the standard biotin-streptavidin affinity model. The samples were analyzed using ellipsometry (SOPRA SE-5, France) and X-ray photoelectron spectroscopy (XPS; Scientific Theta Probe, UK). The morphology of the samples were investigated by atomic force microscopy (AFM; Veeco Dimension 5000 scanning probe microscope). In order to observe the biotin-modified CdQD distribution on PBLA at

collapsed and stretched state, the samples with varying thickness were prepared by overnight incubation. Subsequently, the solvent was removed from the samples by drying in the vacuum freeze dryer (BENCHTOP 2 K; VIRTIS; America) for 10 min at −40 °C. After lyophilization, various analytical tools were employed for characterization of the prepared PBLA-CdQD. Each sample was subjected to ellipsometric data measurements using the modifications performed in the earlier step as a reference for the next step. The refractive indices calculated for the silicon substrate, native Si layer, PGMA brushes, and CdQD at 633 nm were 3.858, 1.4598, 1.353, and 2.53, respectively. Moreover, the distribution of CdQDs attached to PBLA was studied using 100 mW operating Ar blue laser at 488 nm wavelength LSCM (laser scanning confocal microscope; Leica TCS SP5 Confocal Spectral Microscope Imaging System). Jasco FP-500 spectrofluorometer was used to investigate photoluminescence (PL) of the CdQDs. The particle sizes were analyzed by DLS (dynamic light scattering; Zetasizer, Nano-Zs90).

2.2. Development of model and hybrid method

Fig. 1 depicts the schematic representation of the grating structure appraised in this study. It was observed that the top opaque surface of the Si substrate was grafted with binary PGMA. It is important to note that Si was selected as the grating/substrate material particularly due to its light weight, inherent stability, and widespread applications in devices. The geometry of the grating structure is defined by the period (P), grating thickness (h) and grating ridge width (w). As per the opaque object energy balance equation, the value of absorbance is equal to the subtraction of reflectance (R) from unity.

In the current analysis, it was assumed that the incident light is in a wave plane at an orientation defined by the surface normal (z) through free space and the polar angle between the wave vector (k). In addition, the plane of incidence is considered to be one which has both the incident light and the surface normal. Only the x–z plane was considered for a simplified analysis. The Lorentz-Drude model was used to analyze the grating structure optical response and describe the wavelength-dependent dielectric function ε of PBLA-CdQD as below [10,11]:

$$\varepsilon(\omega) = \varepsilon_{r,\infty} + \sum_{k=0}^{K} \frac{f_k \omega_p^2}{\omega_k^2 - \omega^2 + j\omega\Gamma_k} \quad (1)$$

where, $\varepsilon_{r,\infty}$ = optical dielectric constant at an infinite frequency; $\omega = 2\pi c_0/\lambda$ = angular frequency with λ being the wavelength of light in vacuum and c_0 being the speed, respectively; ω_p = plasma frequency, ω_k = resonance frequency, f_k = strength and Γ_k = dampening frequency of the k^{th} oscillator. As shown in Fig. 1, the grating structure is optimized by using the parameters such as filling factor (f), grating period (P), and grating thickness (h). In the current study, the change in experimental grating thickness conforms to theoretical principles. The maximum subwavelength grating period has been defined in a present report [37]. Correspondingly, the range of $0 < f < 1$ is defined by geometric constraints for the filling factor. Lastly, the grating thickness is set by the thickness-to-period ratio at $0.1 < h/P < 1$, in consideration of both deep and shallow gratings.

3. Results and discussion

3.1. Characterization of biotin modified CdQDs

The crystal structure and crystallite size information can be assessed from the X-ray diffraction pattern. Fig. 2a shows the 2θ value peaks at 26.53°, 43.70°, and 51.81° corresponding to the diffraction planes of (002), (110), and (112), respectively. CdS belongs to the hexagonal wurtzite phase with the lattice constants of a = b = 4.140 Å and c = 6.709 Å which concurs with the standard JCPDS card number 89–2944 [38]. Moreover, the diffraction peak broadening is strongly related to the crystallite size. Generally, the decreasing of the particle size leads to peak width increase and vice versa. The broadened diffraction peaks of the prepared sample prove them to be nano-sized crystallites. The CdS nanocrystal values of the crystallite size (S), strain (τ) and dislocation density (δ) were calculated by using the Eqs. (1)–(3) respectively as shown below [39],

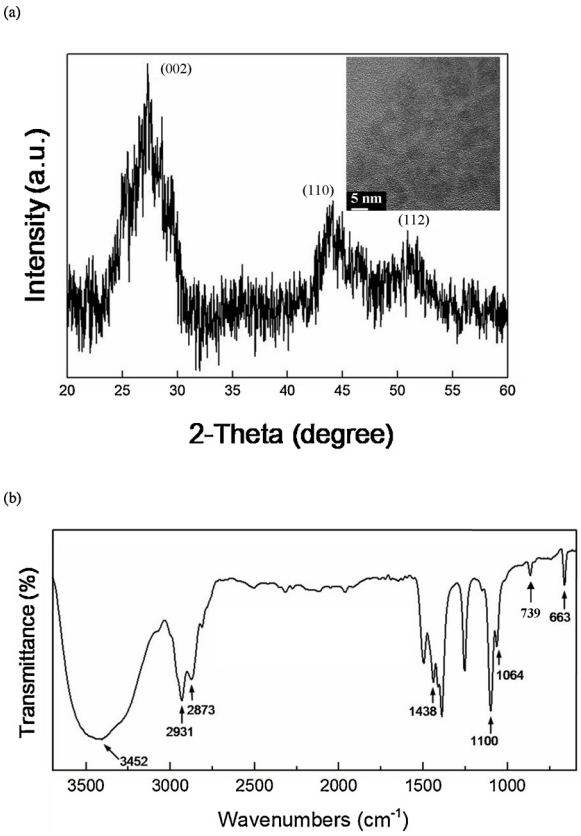

Fig. 2. (a) XRD pattern of biotin modified CdQDs. Insert represents TEM image of biotin stabilized CdQDs. (b) FTIR spectrum of biotin modified CdQDs.

$$S = \frac{0.9\lambda}{H\cos\theta} \quad (2)$$

$$\tau = \frac{H\cos\theta}{4} = \frac{0.9\lambda}{4S} \quad (3)$$

$$\rho = \frac{1}{S^2} \quad (4)$$

where, θ = angle of diffraction, H = full width at half maximum (FWHM) of diffraction peak, and S = crystallite size. XRD is commonly employed to calculate the value of crystallite size and it was found to be 4.36 nm by using Scherrer's formula given as Eq. (2). We propose that biotin has more influence in the attainment of crystallite size reduction of CdS. Fig. 2a inset shows the TEM micrograph of CdS nanoparticles. TEM is a more valuable tool in characterizing the number of crystallites or grains employed in particle formation. The TEM micrograph exhibits spherical morphology with small aggregation of CdS nanoparticles with an average particle size of 4.47 nm. The calculated interplanar spacing (d) from the lattice fringes is 0.34 nm which concurs with the (002) plane of the hexagonal wurtzite phase of CdS [40]. The CdS quantum dots average particle size is projected to be 4.410 ± 0.063 nm. This is in strong correlation with the calculated average crystallite size using XRD and TEM. The calculation of lattice strain gives information about crystal imperfections in terms of lattice dislocations. In other words, it is a measurement of lattice constant distribution. The major strain arises from grain boundary triple junction, sinter stresses or contact, coherency stresses, and stacking faults. By using relation (3), the lattice

strain (τ) was estimated to be 0.749×10^{-3}. The dislocation density (ρ) was calculated for the overall number of defects present in the sample. ρ is commonly expressed as the length of dislocation lines per unit size and found as 0.043 nm/nm^3 by using relation (4) [39]. The crystallite size is inversely proportional to both parameters. This implies that the defects are closely related to the smaller crystallite size of nanoparticles [41]. Fig. 2b shows the Fourier-transform infrared resonance spectroscopy (FTIR) spectrum of biotin-stabilized CdS quantum dots. The signal observed at 3452 cm^{-1} can be attributed to N—H and O—H stretching of biotin on the sample surface. The signals observed at 663 cm^{-1}and 739 cm^{-1} are attributed to the stretching bands of CdS [42]. The signals observed at 1438 cm^{-1} can be ascribed to CH_3 asymmetric bending vibration of methanol. The intense peak observed at 1064 cm^{-1} is due to the C—O stretching vibration of biotin coating and the bands at 2831 cm^{-1} and 2873 cm^{-1} resemble C—H stretching vibration. The above results confirm that the surface of the CdQDs is covered with capping agent.

3.2. Characterization of one-dimensional plasmonic gratings on the surface

The distinguished "grafting from" approach was utilized to investigate the homogeneous distribution of the PGMA brushes prepared on a silicon substrate. It was recognized that the numerous stages could be utilized as an extensive anchoring layer for grafting of a multiplicity of polymer brushes on a silicon substrate. Moreover, XPS was used to analyze the chemical composition of the surfaces at numerous stages during modification of the surface method followed in our previous studies [28,43]. Table 1 summarizes the chemical composition during each stage of surface modification, according to XPS survey spectra. The [C]/[O] ratio values of 0.48 obtained from XPS analysis for Si-PGMA surface agrees well with the theoretical ratio (3/7). Moreover, XPS shows that the [Cd]/[C] and [S]/[C] ratios of Si-PGMA-CdQD surface to be nearly 0.1. These results confirm the formation of PGMA-CQD polymer brush.

Fig. 3 shows 2D and 3D, line cross-section survey and AFM topographic images of the line array of PBLA and PBLA-CdQD with and without streptavidin incubation at 50 nM. The PGMA is grafted as line arrays through ATRP from the bottom surface of trench arrays photoresist. As observed in Fig. 3a, the PBLAs were fabricated successfully, which occurred on the surfaces of Si as a dense characteristic overlayer structure, with line scales equal to 1.5 μm, inside a scanning area of 20 μm × 20 μm. This irregular hill-like structure is revealed in the grafting of PGMA brushes in lines, to the trenches of 1.21 μm and 2.15 μm width at top and bottom, respectively. The hill-like structure could be ascribed to polymer chains collapsing due to narrow grafting sites. Polymer brush collapse and inaccuracy of lithography, scale of these spaces, widths, and grating periods result in imperfect match with the trench scale of photoresist. In addition, the line patterns of PGMA brushes have uniform height (414 nm) and space (309 nm) among the lines. Furthermore, the space between lines represents the polished silicon surface that predominately reflects the incident light to generate diffraction. In addition, the grating period (P) is ca. 2.45 μm, which is the sum of width and space. The irregular hill-like structure is more obvious after immobilization of CdQD on the PBLA chains. The top and bottom widths of the hill-like structure are 1.49 μm and 2.78 μm in the 2.5 μm of grating period, respectively (Fig. 3b). The height of the PGMA-CdQD increased significantly from ca. 414 nm to 984 nm, indicating the ca. dozens of biotin-modified CdQD particles embedded onto the PGMA chains. Fig. 3c reveals the structure of PBLA-CdQD after streptavidin incubation at 50 nM for 2 h. The height of the brush shrunk significantly from 984 nm to 332 nm. Inoculation of streptavidin on the surface induced the assembly of these biotin-modified CdQDs on the polymer chains resulting in the significant collapse of the brushes. Apart from the increase in height, there was no significant change in geometrical parameters (e.g., filling factors and widths) in the grating, after streptavidin incubation.

3.3. Optical properties of PBLA-CdQD

Fig. 4a shows the UV–vis absorbance spectra of free CdQDs, PBLA, PBLA-CdQD with and without streptavidin incubation at 50 nM. It is clearly seen that a strong absorbance band is observed for free CdS at 396 nm and it is highly connected to the innate band gap absorption. The band gap energy value of CdQD is estimated to be 3.13 eV. Electromagnetic wave absorbers are classified into two types, resonant absorbers and broadband absorbers. The crossed grating absorber is a well-known kind of resonant electromagnetic wave absorber which uses a reflective plane with a deep periodic grid [44]. For generating resonance, there is interaction between incident radiation and periodic grid resulting in a period of anomalous diffraction. This absorber displays irregular diffraction which correlates to periods of enriched absorbance [26]. Fig. 4a shows the effect of changes in the height on the absorbance spectra of the PBLA, PBLA-CdQD with and without streptavidin incubation. However, there is no effect on the value of the absorbance peak and FWHM even though the grating height improved from 414 nm to 948 nm, continuing over a constant grating period. PBLA exhibited an absorbance peak at 441 nm, which can be considered as a resonant absorber. The absorbance peak shifted to 396 nm upon increasing the grating height before streptavidin incubation, moving closer to the location of the absorbance peak of CdQDs. The absorbance peak shift to 536 nm following streptavidin incubation at 50 nM was due to the collapse of polymer brush. Each slit in the grating function was a quasi-point source which resulted in the propagation of light in all directions when a normal incidence plane wave travelled through the resonant absorber. Later, the light interacted with the resonant absorber, and the absorbed light was collected as the sum of the interfering wave components, emanating from each slit in the grating. The travelling of diffracted light at any slit in the space resulted in changes in path length to each slit in the grating. The variation in path length affected the wave phases on the point from both slits, thus subtracting or adding to the generation of peaks due to additive interference and valleys due to destructive interference. Specific absorbance

Table 1
Chemical compositions (from XPS core-level spectral area ratios), surface parameters (surface conversion, *Sc*; grafting distance, *Dg*; grafting density, *σ*) on Si-OH, Si-AS, Si-AS-BB, Si-PGMA, Si-PGMA-CdQD films. The data were obtained from three repeated experiments ($p < 0.01$).

Sample	Chemical composition[a]					Surface parameters		
	[O]/[C]	[N]/[C]	[Br]/[C]	[Cd]/[C]	[S]/[C]	*Sc*[b] (mg/m^2)	*Dg*[b] (nm)	*σ*[b] (nm^{-2}) ×10^{-3}
Si-OH	2.48 ± 0.17	–	–	–	–	–	–	–
Si-AS	1.11 ± 0.09	0.29 ± 0.01	–	–	–	0.436 ± 0.03	29.1 ± 1.4	1 ± 0.06
Si-AS-BB	0.51 ± 0.03	0.14 ± 0.01	0.11 ± 0.02	–		0.549 ± 0.03	36.9 ± 2.9	1 ± 0.08
Si-PGMA	0.48 ± 0.03	0.012 ± 0.006	0.013 ± 0.003	–	–	327.8 ± 21.4	8.1 ± 0.6	1.5 ± 0.11
Si-PGMA-CdQD	0.39 ± 0.02	0.09 ± 0.004	–	0.09 ± 0.004	0.11 ± 0.01	795.3 ± 44.1	5.9 ± 0.3	2.8 ± 0.24

[a] Determined from XPS core-level spectral area ratio.

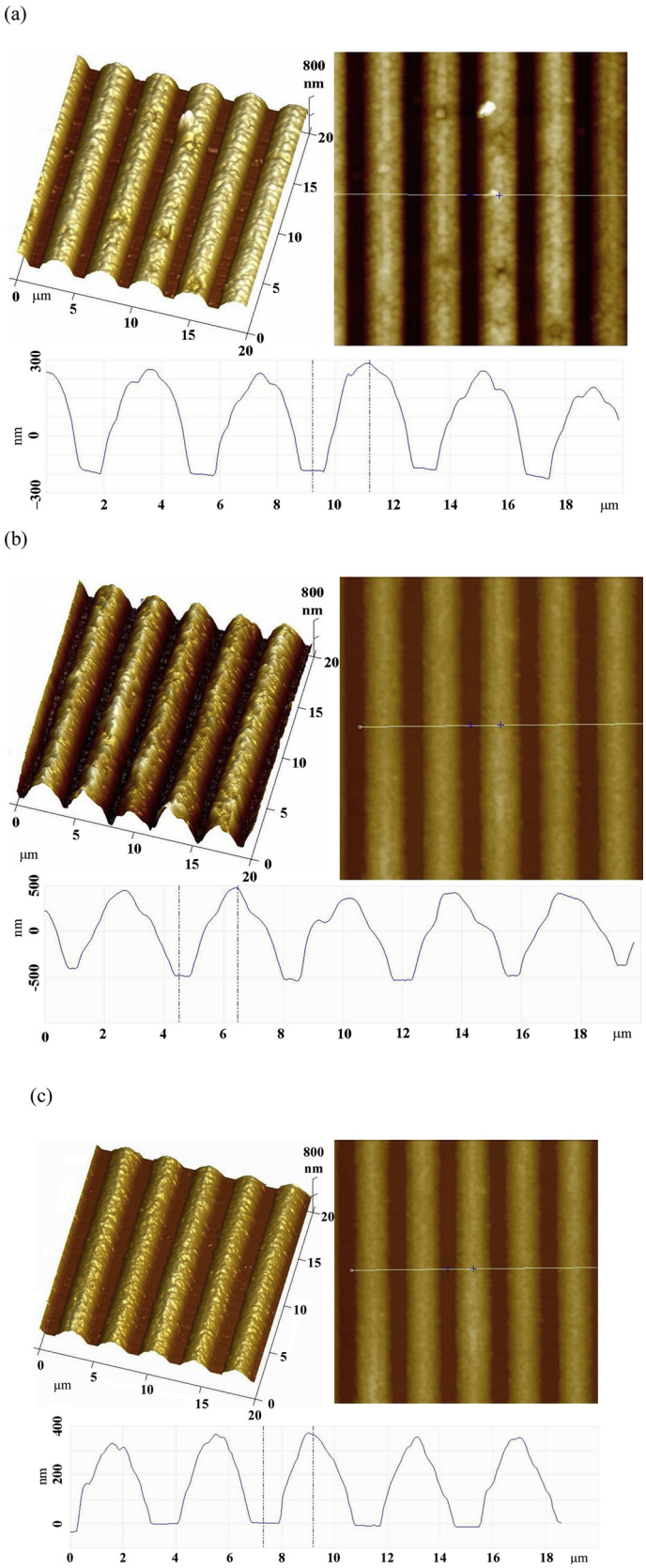

Fig. 3. 2D and 3D AFM height images (20 µm × 20 µm) of liner arrays of (a) bare PBLA, PBLA-CdQD (b) without and (c) with streptavidin incubation at 50 nM.

of the plasmonic grating is expected to enhance the photoluminescence of CdQDs. There have been wider studies on the physical mechanism of enriched micro/nanostructures underlying transmission/absorbance [45,46]. The physical mechanism confirmed that grating structures occur either due to a RW (Rayleigh-Wood anomaly) [47], or surface SPPs (plasmon polaritons) [48]. These resonance excitations are

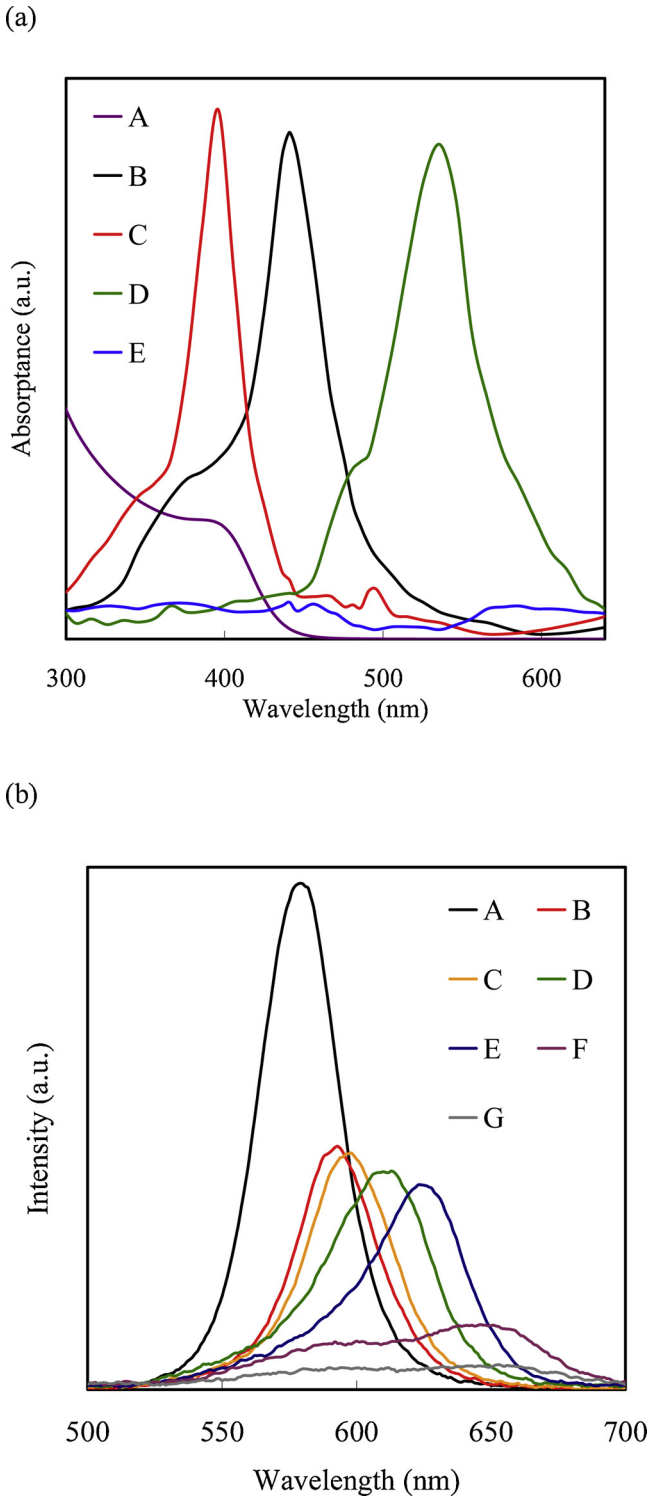

Fig. 4. (a) UV–vis diffuse reflectance absorption spectra of free CdQDs (A), PBLA(B), PBLA-CdQD without (C) and with streptavidin incubation at 50 nM (D). (b) PL emission spectra of free CdQDs (A), PBLA (B), PGMA-CdQD without (C) and with streptavidin incubation at 25 (D), 50 (E), 75 (F), and 100 (F) nM, and planar PGMA-CdQD (G). (For interpretation of the references to colour in the text, the reader is referred to the web version of this article.)

effective for TM waves conferred as follows:

The appearance or disappearance of diffraction orders at grating order induces the RW anomaly process with abrupt changes in sub-wavelength grating structures in terms of reflective, transmittance and absorbance.

$$\left(\frac{\lambda}{P}j\right)^2 + 2\frac{\lambda}{P}\sin\theta - \cos^2\theta = 0 \tag{5}$$

where, P = grating period; λ = incident wavelength; j = diffraction order, and θ = angle of incidence. SPPs are defined as electromagnetic waves combined with charge oscillations of free electrons propagating along the interface. The expressions for SPP excitation is given below [26]:

$$n_d \sin\theta + j\frac{\lambda}{P} = \pm\sqrt{\frac{\varepsilon_m n_d^2}{\varepsilon_m + n_d^2}} \tag{6}$$

where, θ = angle of occurrence and ε_m and n_d are permittivity (i.e., PBLA-CdQD in the current case) and the refractive index of air (n_d = 1), respectively. Moreover, λ is the wavelength (i.e., 200–800 nm in the current case) and j is an integer indicating the diffraction order. Eventually, the " ± " sign corresponds to the diffraction orders of $j > 0$ and $j < 0$, correspondingly.

Photoluminescence (PL) emission spectra were also utilized to analyze the enhancement of CdQD fluorescence with grating structure. Normally, the PL peak with higher and lower intensity represents the rapid charge recombination, and charge separation respectively [49]. Fig. 4b shows PL spectra of free CdQD, PBLA-CdQD with streptavidin incubation at 25, 50, 75, 100 nM and planar PGMA-CdQD with streptavidin incubation at 100 mM. The observation of a sharp peak at 580 nm PL spectrum matches with the previous report regarding CdQDs [50]. It can be attributed to a band-to-band emission of free CdQDs without immobilization on a PBLA layer. Immobilization of CdQDs on the PGMA chains decreased the freedom of CdQDs resulting in the red-shift of the fluorescence peak from 580 nm to 593 nm. After streptavidin incubation at 25 nM, the fluorescence peak slightly red-shifted from 593 nm to 598 nm, indicated that the streptavidin incubation varied the line patterns slightly. The fluorescence peak further blue-shifted from 598 nm to 652 nm upon increasing the concentration of streptavidin from 25 to 50 μg/ml. The red-shift increased with the concentration of streptavidin, while the intensity decreased with the concentration of streptavidin. The results show that streptavidin incubation induced assembly of CdQDs on the PGMA chains resulting in the significant red-shift of the absorbance peak deviated from the absorbance peak of PBLA, ranging from 396 nm to 536 nm. PBLA did not provide sufficient absorbance to excite the CdQD efficiently resulting in the decay of PL intensity emission. Location of the absorbance peak of PBLA matching well with that of the CdQD, implies enhanced charge carrier recombination rate. The PL results further show that combining PBLA with CdQD to form a composite could be promising for the holes under light irradiation and separation of photogenerated electrons. The planar PGMA-CdQD did not exhibit an obvious PL emission, verifying that the grating structure enhanced the PL emission of QDs substantially. In addition, BSA and AGRI were exploited to examine the selectivity of the PBLA-CdQD at 100 nM. Both red-shift and intensity could not change considerably with AGRI or BSA concentrations. The results show that PBLA-CdQD could detect streptavidin accurately with high selectivity. Fig. 5 displays the LSCM images of these PBLA-CdQD gratings before and after streptavidin incubation at 50 nM. The apparent line arrays of red luminescence with 1.5 μm resolution represent good immobilization of CdQDs on PBLA. The immobilization of CdQDs on the polymer brushes have been recognized by exploiting the covalent bonding between epoxy functionalities of PGMA and surface functionalities (-NH groups) of CdQDs [51–53]. Furthermore, efficient dispersion of the CdQDs onto the incubated aqueous solution results into their homogeneous spreading onto the PGMA brushes. Fig. 5a shows that the fluorescence intensity of red luminescence decayed significantly after streptavidin incubation at 50 nM due to the deviation of absorbance of CdQDs from that of PGMA gratings. When the streptavidin bound to biotin-modified CdQD on the PBLA, a change in the effectual refractive index value of gratings was anticipated owing to the high refractive index of CdQDs. The line patterns of PGMA-CdQD

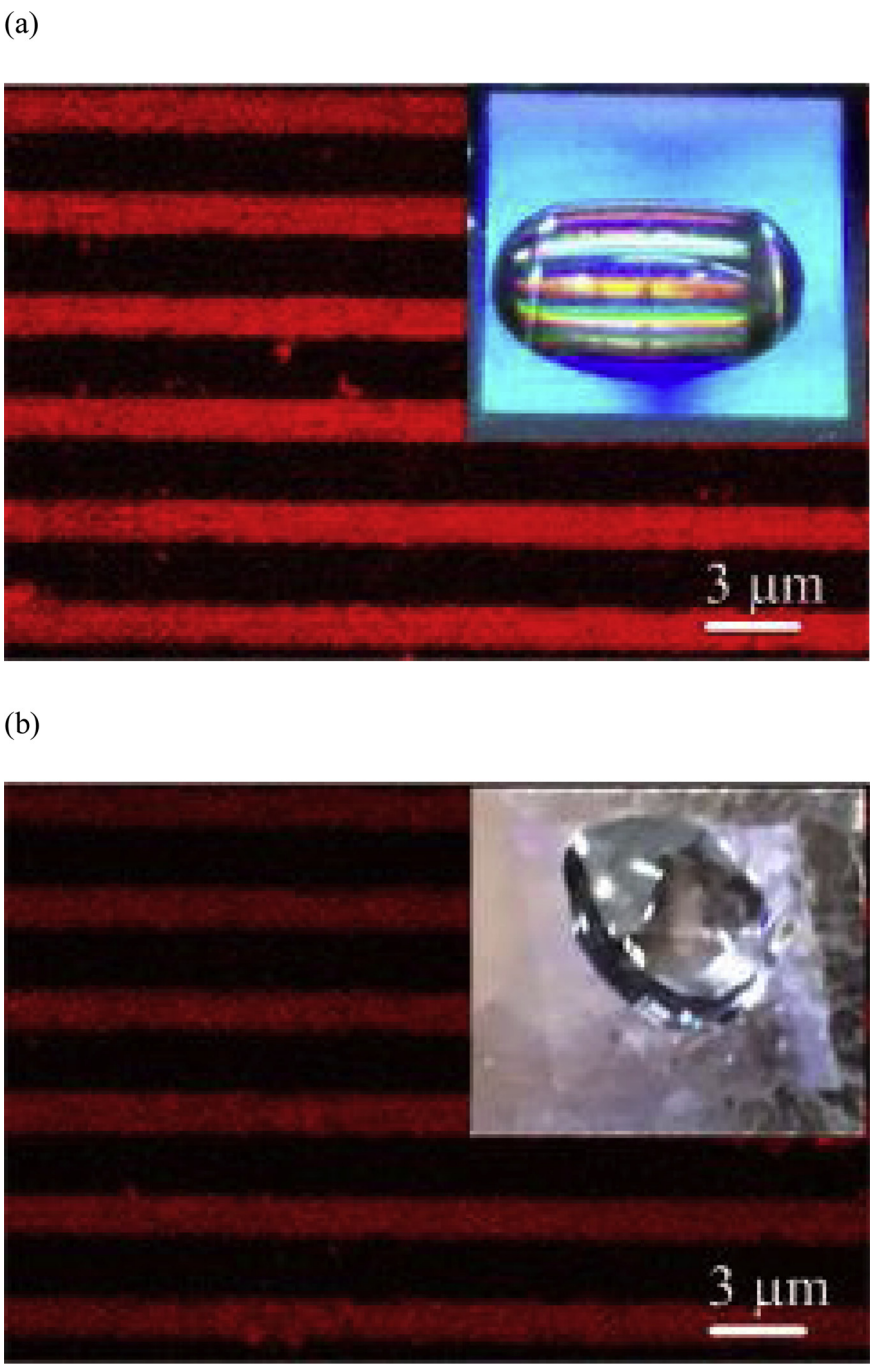

Fig. 5. LSCM images of PBLA-CdQD (a) without and (b) with streptavidin incubation at 50 nM. Inserts represent their photographs. (For interpretation of the references to colour in the text, the reader is referred to the web version of this article.)

brushes exhibit blue color, with varying effective refractive indices for the TE and TM polarizations on the surface (Fig. 5a insert). For our plasmonic grating, the n_{eff} for TE and TM polarizations were perpendicular and parallel, corresponding to the line-patterned brushes. The blue color turned to light purple color after streptavidin incubation at 50 nM, indicating that the diffractive reflects weakened the intensity of PBLA-CdQD with assembly of CdQDs. As per color change, and n_{eff} of the streptavidin-responsive PBLA-CdQD, we calculated the refractive index of the PGMA-CdQD thin film at 633 nm to be 1.584 (standard value) by using ellipsometry. Grafting of the PGMA-CdQD was performed as the grating decreased the effective refractive index value from 1.584 to 1.313. CdQDs with high refractive index (2.476) can absorb within the PGMA to increase the effective refractive index of the PGMA thin film. The effective refractive index of the PGMA-CdQD thin film after streptavidin incubation at 50 nM is nevertheless, roughly 1.737. This small change from 1.584 to 1.737 is difficult to recognize by naked eye. The linear structure amplified the difference in refractive index before and after streptavidin incubation, facilitating color changes that can be witnessed by the naked eye, due to diffractive reflection effects. Overall, the result shows that the geometry of the single-layered PBLA-CdQD can be effortlessly tuned to attain an intensity range of PL properties. The above observations strongly suggest that fabricated nanosensors could sense the nature of the surrounding media such as in microfluidic devices, from dispersing to the assembly state and vice versa, as well as various solvent media.

4. Conclusions

In summary, we have used a “grafting from” method with ATRP to prepare well-defined PBLA on Si wafers. It provides the patterned polymer/quantum dot composite thin films as plasmonic grating absorber of nanoscale dimensions. PBLA with absorbance peak at 396 nm of wavelength could significantly enhance the fluorescence of CdQDs at 395 nm through effects of SLRs and LSPRs when absorbance peak of quantum dots is similar to that of plasmonic absorbers. The fluorescence decays with streptavidin incubation indicate that assembly of CdQD on the PGMA chains results the change in geometry of the grating as well as absorbance peak. The PBLA-CdQD grating has been used for the fabrication of biosensors by exploiting streptavidin-induced coiling-stretching of polymer brushes and tunable fluorescent properties of PBLA-CdQD. The employed approach can be applied to effectively modify the surface of grating through immobilization and is also versatile in nature. The same methodology can be satisfactorily employed for any biological application for inducing switching of bioactive agents through the surface modification of polymer brushes.

Acknowledgments

We sincerely thank the National Nano Device Laboratory for its financial support of the electron beam lithography system, and the Ministry of Science and Technology of Taiwan, Republic of China, under project numbers: MOST106-2221-E-011-135-MY3. This work was financially supported by the Applied Research Center for Thin-Film Metallic Glass from The Featured Areas Research Center Program within the framework of the Higher Education Sprout Project by the Ministry of Education (MOE) in Taiwan.

References

[1] M. Thambidurai, N. Muthukumarasamy, S. Agilan, N. Murugan, S. Vasantha, R. Balasundaraprabhu, T.S. Senthil, J. Mater. Sci. 45 (2010) 3254–3258.
[2] J. Kim, H.J. Shim, J. Yang, M.K. Choi, D.C. Kim, J. Kim, T. Hyeon, D.-H. Kim, Adv. Mater. (2017) 1700217.
[3] H.-M. Kim, D. Geng, J. Kim, E. Hwang, J. Jang, ACS Appl. Mater. Interfaces 8 (2016) 28727–28736.
[4] C.R. Kagan, E. Lifshitz, E.H. Sargent, D.V. Talapin, Science 353 (2016) aac5523.
[5] Q. Lin, F. Chen, H. Wang, H. Shen, A. Wang, L. Wang, F. Zhang, F. Guo, L.S. Li, ACS Appl. Mater. Interfaces 8 (2016) 11557–11563.
[6] F. Zhan, W. Liu, H. Li, Y. Yang, M. Wang, Appl. Surf. Sci. 45 (2018) 476–483.
[7] Y. Liu, Z. Kang, H. Si, P. Li, S. Cao, S. Liu, Y. Li, S. Zhang, Z. Zhang, Q. Liao, Nano Energy 35 (2017) 189–198.
[8] C. Schäfer, D.A. Gollmer, A. Horrer, J. Fulmes, A. Weber-Bargioni, S. Cabrini, P.J. Schuck, D.P. Kern, M. Fleischer, Nanoscale 5 (2013) 7861–7866.
[9] J.K. Chen, G.Y. Zhou, C.J. Chang, A.W. Lee, F.C. Chang, Biosens. Bioelectron. 54 (2014) 35–41.
[10] B. Auguié, W.L. Barnes, Phys. Rev. Lett. 101 (2008) 143902.
[11] V.G. Kravets, F. Schedin, A.N. Grigorenko, Phys. Rev. Lett. 101 (2008) 087403.
[12] N. Félidj, G. Laurent, J. Aubard, G. Lévi, A. Hohenau, J.R. Krenn, F.R. Aussenegg, J. Chem. Phys. 123 (2005) 221103.
[13] G. Pellegrini, G. Mattei, P. Mazzoldi, J. Phys. Chem. C 115 (2011) 24662.
[14] G. Vecchi, V. Giannini, J. Gómez Rivas, Phys. Rev. Lett. 102 (2009) 146807.
[15] W. Zhou, M. Dridi, J.Y. Suh, C.H. Kim, D.T. Co, M.R. Wasielewski, G.C. Schatz, T.W. Odom, Nat. Nano 8 (2013) 506.
[16] S.R.K. Rodriguez, J. Feist, M.A. Verschuuren, F.J. Garcia Vidal, J. Gómez Rivas, Phys. Rev. Lett. 111 (2013) 166802.
[17] A.I. Väkeväinen, R.J. Moerland, H.T. Rekola, A.P. Eskelinen, J.P. Martikainen, D.H. Kim, P. Törmä, Nano Lett. 14 (2014) 1721.
[18] J. Chen, J. Qui, S. Fan, S. Kuo, F. Ko, C. Chu, F. Chang, J. Colloid Interface Sci. 367 (2012) 40–48.
[19] J. Guo, Z. Lin, C. Chang, C. Lu, J. Chen, Appl. Surf. Sci. 439 (2018) 313–322.
[20] J.K. Chen, F.H. Ko, C.H. Chan, C.F. Huang, F.C. Chang, Semicond. Sci. Technol. 21 (2006) 1213–1220.
[21] J. Zeng, C. Cheng, B. Huang, C. Huang, J. Chen, Sens. Actuator B 243 (2017) 234–243.
[22] J. Chen, J. Wang, C. Cheng, J. Chang, F. Chang, Appl. Phys. Lett. 102 (2013) 151906.
[23] J.R. Zeng, C.C. Cheng, A.W. Lee, P.L. Wei, J.K. Chen, Microchim. Acta 184 (2017) 2723–2730.
[24] J.K. Chen, J.H. Wang, C.C. Cheng, J.Y. Chang, ACS Appl. Mater. Interfaces 5 (2013) 2959–2966.
[25] G.Y. Zhou, A.W. Lee, J.Y. Chang, C.H. Huang, J.K. Chen, J. Mater. Chem. C 2 (2014) 8226–8234.
[26] J.K. Chen, T.Y. Chen, J. Colloid Interface Sci. 355 (2011) 359–367.
[27] J.K. Chen, J.H. Wang, C.J. Chang, C.F. Huang, Sens. Actuator B 188 (2013) 1123–1131.
[28] V.J. Cunningham, A.M. Alswieleh, K.L. Thompson, M. Williams, G.J. Leggett, S.P. Armes, O.M. Musa, Macromolecules 47 (2014) 5613–5623.
[29] N.J. Warren, J. Rosselgong, J. Madsen, S.P. Armes, Biomacromolecules 16 (2015) 2514–2521.
[30] Z. Xie, C. Chen, X. Zhou, T. Gao, D. Liu, Q. Miao, Z. Zheng, ACS Appl. Mater. Interfaces 6 (2014) 11955–11964.
[31] Q.L. Li, W.X. Gu, H. Gao, Y.W. Yang, Chem. Commun. 50 (2014) 13201–13215.
[32] J.R. Zeng, C.C. Cheng, C.J. Chang, C.H. Huang, J.K. Chen, Dye. Pigm. 139 (2017) 300–309.
[33] T.Y. Chen, J.K. Chen, Colloid Polym. Sci. 289 (2011) 433–445.
[34] H. Kikuta, H. Toyotai, W. Yul, Opt. Rev. 10 (2003) 63–73.
[35] T. Khantaw, C. Boonmee, T. Tuntulani, W. Ngeontae, Talanta 115 (2013) 849–856.
[36] W.T. Chena, S.S. Lib, J.P. Chua, K.C. Fengc, J.K. Chen, Biosens. Bioelectron. 102 (2018) 129–135.
[37] L.C. Botten, M.S. Craig, R.C. McPhedran, Opt. Acta 28 (1981) 1103–1106.
[38] V. Singh, P.J. Chauhan, Phys. Chem. Solids 70 (2009) 1074–1079.
[39] O.H. Abd-Elkader, A.A. Shaltout, Mater. Sci. Semicond. Process. 35 (2015) 132–138.
[40] H. Wang, P. Fang, Z. Chen, S. Wang, J. Alloy Compd. 461 (2008) 418–422.
[41] S. Kumar, P. Sharma, V. Sharma, Electron. Mater. Lett. 9 (2013) 371–374.
[42] M.F. Kotkata, A.E. Masoud, M.B. Mohamed, E.A. Mahmoud, Physica E 41 (2009) 1457–1465.
[43] J.R. Zeng, C.C. Cheng, B.R. Huang, C.H. Huang, J.K. Chen, Sens. Actuator B 243 (2017) 234–243.
[44] J. Homola, I. Koudela, S.S. Yee, Sens. Actuators B 54 (1999) 1624.
[45] S.E. Han, G. Chen, Nano Lett. 10 (2010) 1012–1015.
[46] J.J. Greffet, R. Carminati, K. Joulain, J.P. Mulet, S. Mainguy, Y. Chen, Nature 416 (2002) 61–64.
[47] A. Hessel, A.A. Oliner, Appl. Opt. 4 (1965) 1275–1297.
[48] M.C. Hutley, D. Maystre, Opt. Commun. 19 (1976) 431–436.
[49] S. Ma, J. Xie, J.Q. Wen, K.L. He, X. Li, W. Liu, X.C. Zhang, Appl. Surf. Sci. 391 (2017) 580–591.
[50] B. Chai, M. Xu, J. Yan, Z. Ren, Appl. Surf. Sci. 430 (2018) 523–530.
[51] E.M. Muzammil, A. Khan, M.C. Stuparu, RSC Adv. 7 (2017) 55874–55884.
[52] N.U. Kim, B.J. Park, Y. Choi, K.B. Lee, J.H. Kim, Macromolecules 50 (2017) 8938–8947.
[53] P. Guo, W. Gu, Q. Chen, H. Lu, X. Han, W. Li, H. Gao, J. Mater. Chem. B 3 (2015) 6911–6918.